Stimuli-responsive nanotheranostics intended for oncological diseases: In vitro evaluation of their target, diagnostic and drug release capabilities.

Journal:	*New Journal of Chemistry*
Manuscript ID	NJ-ART-10-2018-005289.R1
Article Type:	Paper
Date Submitted by the Author:	03-Dec-2018
Complete List of Authors:	Azcona, Pamela; Universidad Nacional del Sur, Química; Instituto de Quimica del Sur, Química Montiel Schneider, Gabriela; Instituto de Quimica del Sur, Química; Universidad Nacional del Sur, Química Grünhut, Marcos; INQUISUR-CONICET; Universidad Nacional del Sur, Química Lassalle, Veronica L.; INQUISUR; Universidad Nacional del Sur, Química

New Journal of Chemistry

ARTICLE

Stimuli-responsive nanotheranostics intended for oncological diseases: *In vitro* evaluation of their target, diagnostic and drug release capabilities.

Received 00th January 20xx,
Accepted 00th January 20xx

DOI: 10.1039/x0xx00000x

www.rsc.org/

Pamela Liliana Azcona[a], María Gabriela Montiel Schneider[a], Marcos Grünhut[a], Verónica Leticia Lassalle*[a]

Abstract

Magnetic nanotheranostics were designed from iron oxide nanoparticles (***MNPs***) functionalized with folic acid (***FA***)and loaded with Doxorubicin (***Doxo***) as a therapeutic agent. The ***Doxo*** incorporation was carefully examined to attain satisfactory drug loading efficiency. The magnet-guiding ability was in vitro examined. To do this, a novel continuous flow system was fabricated to quantify the amount of ***MNPs*** retained in the magnet site in an environment and conditions mimicking the bloodstream. The obtained data suggest that almost 21% of the total circulating nanoparticles were accumulated in target site after 45min of assay. Such amount assured the doses of ***Doxo*** commonly employed during *in vivo* studies. ***Doxo*** release was analysed by implementing an original procedure devoted to simulate the pathways followed by ***MNPs*** once intravenous administrated. From these studies, reliable data on the amount of drug that effectively reach the target site was obtained. The efficiency of the nanosystems as selective contrast agents in MRI was analysed using a clinical 1.5T equipment. Their potential as T_2 weighted contrast media was demonstrated. The data collected within this work appear as the former initial stage to validate the nanotheranostics before *in vivo* evaluation of this novel technology.

Introduction

Chemotherapy, radiotherapy and photothermal therapy are the most common treatments for cancer diseases[1–3]. In this regards, Doxorubicin (***Doxo***) is one of the most effective chemotherapeutic antitumor agents used in the treatment of various cancers including leukemia, ovarian and especially late stage breast cancer[4]. Nevertheless, many side effects are associated to the administration of this drug, among which the cardiotoxicity is the most relevant[5]. Another obstacle in chemotherapy is multidrug resistance (MDR) effect which reduces the efficacy of cancer treatments[6]. These unwanted effects are related to large drug dosage, poor selectivity and efficacy associated to the non-specific distribution of drugs in the body. Nowadays nanotechnology may overcome this limitation by offering new and safe platforms for delivery of therapeutic drugs[7]. In recent years, innovative devices that could be simultaneously employed for the treatment and diagnostic of diseases have emerged as very promising alternatives. These nanotechnological tools, defined as theranostics, are proposed to combine imaging functionalities, such as magnetic resonance (MRI), with therapeutic agents in a unique device[8]. In this concern, it would be possible to obtain data of an initial diagnosis and monitoring the progress of the pathology in real time while the treatment is taking place. This is an interesting advantage considering that information on the efficiency of a medical treatment may be further achieved[9].

Magnetic nanoparticles (***MNPs***) based on iron oxides, result attractive for the design of theranostics with improved properties due to their magnetism (or superparamagnetism), biodegradability, relatively low toxicity and capability to generate contrast in MRI[10]. Furthermore, these nanodevices offer the possibility to conveniently modify their surface to loading several therapeutic agent and/or active biological molecules to assess the therapeutic or target function[10]. Schleich et al. synthesized PLGA-based nanoparticles loaded with paclitaxel and superparamagnetic iron oxides grafted with the tripeptide arginine–glycine–aspartic acid (RGD) on their surface. They aimed to evaluate different strategies in terms of targeting of nanodivices; and found that the modification with RGD improves their properties in terms of selectivity and magnetic combined targeting[11].

The aim of this contribution is to attain an efficient nanotheranostic with suitable properties for its future application in the diagnostic and therapy of oncological diseases. Magnetite nanoparticles functionalized with folic acid were loaded with the oncological drug ***Doxorubicin***. Aspects related to the drug loading and release procedures are addressed. Although several articles referring to magnetic nanoparticles loaded ***Doxo*** are currently

[a] *INQUISUR, Departamento de Química, Universidad Nacional del Sur (UNS)-CONICET, Av. Alem 1253, 8000 Bahía Blanca, Argentina.*

**Corresponding author: Verónica Lassalle*
E-mail addresses: veronica.lassalle@uns.edu.ar, (V. Lassalle). Tel. +54 0291 4595101 ext. 3534.

Electronic Supplementary Information (ESI) available: [details of any supplementary information available should be included here]. See DOI: 10.1039/x0xx00000x

found in the literature[12], the present contribution provides additional knowledge and information in several points. One of them is related to the release study. Here, the release was analyzed by implementing an original procedure devoted to simulate the pathways followed by ***MNPs*** once intravenous administrated. Besides, the evaluation of ***MNPs*** ability concerning the magnetic guide and accumulation in the target site was assessed. In this concern, this work proposes a practical and novel continuous flow system to estimate the magnetic stimuli active targeting capability of ***MNPs***. To the best of these authors knowledge, very few articles are actually found in open literature dealing with the use of *in vitro* flow like systems to assess the magnet affinity[13–15]. Instead, *in vivo* experiments are currently employed to this end[16,17].

From the achieved data, an integral analysis on the real potential of these magnetic nanodevices as theranostics has been obtained covering all the interest aspects, i.e. therapeutic, diagnostic (by MRI) and target capabilities. The information recompiled within this manuscript, even as *in vitro*, is considered highly useful as the former stage, before designing future *in vivo* pre-clinical assays.

Experimental

Materialsand methods

Materials

All reagents and solvents were of analytical grade. Ferric chloride hexahydrate (99.99%) and sodium dodecyl sulfate (SDS) were provided by Biopack (Argentina). Ferrous sulphate heptahydrate (99.99%) was provided by Mallinckradt Chemical Works (USA). Sodium hydroxide and acetic acid (29%) were purchased from Cicarelli (Argentina). Absolute Ethanol was provided by Quimicor (Argentina). (3-Aminopropyl) triethoxysilane (APTS) was provided by Avocado Research chemicals (United Kingdom). N,N'-dicyclohexylcarbodiimide (DCC) was purchased from Fluka (Germany). Folic Acid (FA) and Dimethylsulfoxide (DMSO) were purchased from Sigma Aldrich (Germany). Commercial Doxorubicin was provided by IMA Laboratories (Argentina) and donated by the Hospital Provincial of Neuquén (Neuquén, Argentina). Bidistilled water (BW) with conductivity about 5.00 µS was employed.

Methods

Synthesis of magnetic nanocarriers MNPs@FA

Synthesis of stabilized magnetic core. The magnetic core of magnetite (MAG) was prepared following previous own reported protocol[18]. Briefly, 5.401g of $FeCl_3.6H_2O$ (0.02 moles of Fe^{3+}) and 2.807g of $FeSO_4.7H_2O$ (0.01 moles de Fe^{2+}) and 0.0027 moles of SDS were dissolved in 100mL of BW. This mixture was added to an alkali solution of NaOH 5 mol.L-1 in a controlled way. This process rendered a dark solution and the solid was decanted using a magnet. The supernatant was extracted; and the solid was washed several times with BW and eventually ethanol. Washings were repeated until both, pH and conductivity, reached the levels corresponding to distilled water. The solid was dried in oven at 45◦C overnight under vacuum.

Coupling of FA. A preliminary treatment with APTS was required in order to achieve the *FA* linked on *MAG* surface. This procedure has been extensively studied in a previous own contribution[19]. In brief, $3.01x10^{-3}$ moles of APTS were added to $1.17x10^{-3}$ moles of ***MAG*** in 75mL of absolute ethanol and stirred for 8 h. The solution was decanted using an Nd magnet and washed several times with absolute ethanol to eliminate the APTS excess. The obtained material was called ***MNPs***. 100 mg of ***FA*** and 36 mg of DCC were dissolved in 5 mL of DMSO and stirred during 30 min at room temperature. After that, 5mL of a dispersion containing 100mg of ***MNPs*** in ethanol was added and the reaction was allowed for 24 h at room temperature under magnetic stirring. Several washes were performed to remove the side-product formed. The obtained formulation was called ***MNPs@FA***.

Adsorption of a therapeutic agent: Doxorubicin.

The loading of ***Doxo*** on ***MNPs@FA*** was achieved using a simple adsorption method, previously reported in the literature with some modifications[20]. Aqueous dispersions of ***MNPs@FA*** were mixed with ***Doxorubicin*** solution ([Doxo] 2mg. mL^{-1}) under magnetic stirring. The final samples were decanted using an Nd magnet, and dried in oven at 34◦C under vacuum. The following nominal Doxo/MNPs@FA mass ratios were explored: 0.5/10, 1/10, and 2/10. The obtained formulations were called ***MNPs@FA-Doxo0.5***, ***MNPs@FA-Doxo1*** and ***MNPs@FA-Doxo2***, respectively. The same protocol was followed, employing a mass ratio 1/10 but fixing the pH at 6. The obtained sample was called ***MNPs@FA-Doxo6***. Finally, the adsorption of ***Doxo*** on ***MNPs*** without ***FA*** was also evaluated (mass ratio 1/10) and the sample was named ***MNPs@Doxo***. UV-visible spectroscopic measurements at 480 nm were carried out to determine the amount of drug incorporated on ***MNPs@FA***[21].
The drug loading efficiency (% DLE) and drug loading capability (% DLC) of the nanocarriers were calculated as follows:

$$\%\mathrm{DLE} = \left(\frac{\mathrm{W1}}{\mathrm{W3}}\right)\mathrm{x}\ 100$$

$$\%\mathrm{DLC} = \left(\frac{\mathrm{W1}}{\mathrm{W2}}\right)\mathrm{x}\ 100$$

Where W1 represents the total amount of drug in the ***MNPs@FA***, W2 is the total mass of ***MNPs@FA***, and W3 indicates the total initial mass of ***Doxo***.

Kinetic of drug adsorption. 50 mg of ***MNPs@FA*** were mixed with 2.5 mL of ***Doxorubicin*** solution. Aliquots of the supernatant were withdrawn at 3, 4, 5, 6, 7, 8, and 24h during the reaction advance. The remained drug content in the supernatant was measured by UV–Vis spectroscopy at 480 nm. The solid was decanted by means of Nd magnet after 24 hours of reaction, and dried in oven at 34◦C under vacuum.

Characterization

Hydrodynamic diameter (HD, nm) and Z potential (ζ), mV) measurements were performed in a Malvern Zetasizer equipment; operating with He Ne gas laser, at wavelength 633 nm, with data collection time of already 70s. The dispersions were prepared in distilled water. The informed values were an average of about five-seven repeated measurements. The size measurements were expressed as number distribution.

Transmission infrared Fourier transform spectroscopy (FTIR) was employed using a Thermo Scientific Nicolet iS50 NIR module with Integrating Sphere in the frequency range 4000-400 cm^{-1}.

The UV-visible and turbidimetric measurements were performed on a spectrophotometer Agilent Technologies 8453 A.

Atomic absorption spectroscopy was assessed using a GBC Avanta 932. Morphological characterization was achieved bytransmission electron microscopy (TEM, JEOL 100 CX II, Tokyo, Japan).

Preliminary in vitro target assay

A continuous flow system (FS) with a target magnetic point (TMP) was designed and implemented. The system was consisted of one channel (Teflon®; 0.8 mm i.d.) where by ***MNPs@FA*** suspension flowed at 0.30 mL min^{-1} during 45 min by activation of a peristaltic pump (Gilson minipuls 3) which operated at 5 rpm with a Tygon® tube (0.76 mm i.d.). A magnet of 5x3mm (diameter and thickness, respectively) and 0.3 Tesla (T) of power was placed on a point of the channel at 1mm of distance of the flow. This magnet constituted the TMP (See Scheme 1).

After passed through TMP, the flow was pumped toward a UV-visible flow cell (Hellma, 18 µl) coupled to spectrophotometer (Agilent Technologies 8453A). On this form, the retention of the ***MNPs@FA*** on the TMP was monitored on-line by turbidimetric measurements at 440 nm and as a function of the assay´s time. A stirring system was implemented in order to avoid the aggregation of the ***MNPs@FA*** during the assay period. The stirring system was assembled on top of the flask containing the sample and was done by coupling a PTFE blade vertically to a microprocessor ventilator (Intel®, DC 12 V, 28 G-forces). On the other hand, the temperature of the sample was maintained at 37ºC by means of a ceramic plate (Raid® plug-in mosquito, 220 V) placed on the bottom of the flask (Scheme 1). The FS was a closed system; therefore, the ***MNPs@FA*** suspension was recycled toward their flask during the experiment.

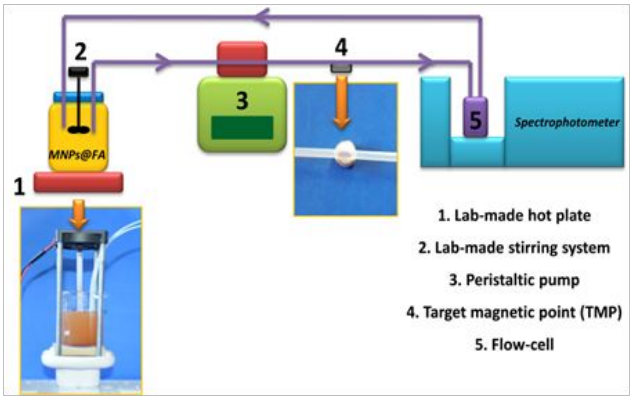

Scheme 1. Continuous flow system implemented for the study of retention of ***MNPs@FA*** under the influence of a magnetic field. The photos show the stirring and heating systems (on the left) and the target magnetic point (on the right). The arrows indicate the direction of the flow (0.30 mL min^{-1}).

Additionally, at the end of the assay the accumulated ***MNPs*** were recovered and the Fe content measured by atomic absorption spectroscopy (AAS). The targeting efficiency or ***MNPs*** accumulation efficiency was calculated as follows:

$$\%TE = \left(\frac{Fe\ 1}{Fe\ 2}\right) x\ 100$$

Where ***Fe1*** represents the amount of Fe retained in the target place at the end of the assay and determined by AAS; and ***Fe2*** means the total mass of Fe that circulated through the target site during the test time.

Magnetic Resonance Imaging (MRI)

The potential of the synthesized nanoparticles as MRI contrast agents (CA) was evaluated using a clinical whole-body scanner (Phillips Achieva 1.5), employing a spin echo (SE) pulse sequence. A series of dispersions of ***MNPs@FA*** and ***MNPs@FA-Doxo*** (0.0 to 0.4 mM Fe) were prepared in aqueous media and T_2 weighted images were acquired at different times echo (TE) (80 to 500 ms), while time repetition was kept constant at 4000 ms.

In vitro Doxorubicin release

12 mg of *MNPs@FA-Doxo* were firstly dispersed in 12 mL of phosphate buffer saline (PBS), pH 7.4 and incubated at 37°C under magnetic stirring during 1 h. Samples were withdrawn at prefixed times (15, 30, 45, and 60 min.) and filtrated in order to obtain a clean solution to analyse the drug content by UV-visible spectroscopy. After that, the PBS buffer was replaced for acetate buffer, pH 4.9 aiming to simulate the endosomal/lysosomal media in a tumoral environment. The suspension was keeping at 37°C under magnetic stirring during 4 h. In this second step of the experience, samples were withdrawn and filtrated every hour and the drug content was analysed by UV-visible spectroscopy. In Scheme 2, the entire procedure is presented.

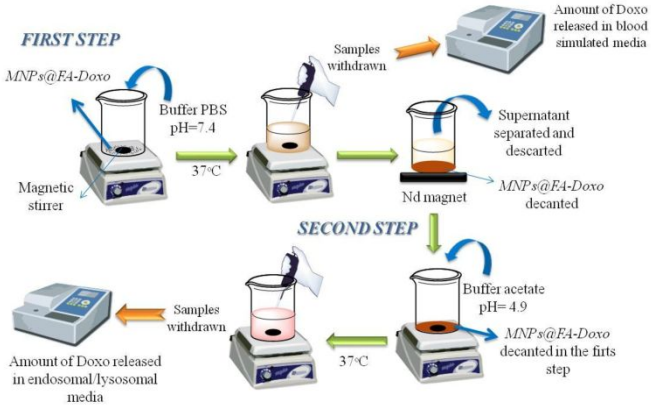

Scheme 2. Steps involved in ***Doxo*** release study.

Results and discussion

Physicochemical characterization of MNPs@FA-Doxo

An exhaustive characterization of ***MAG***, ***MNPs*** and ***MNPs@FA***, regarding to their crystalline structure (by XRD), magnetic properties (by VSM), FTIR and UV spectroscopy, DLS, ζ, and TGA was earlier developed and reported in own previous works[18,19] .

FTIR was employed to confirm the adsorption of ***Doxo*** on ***MNPs@FA*** surface. Fig.1a and b compare FTIR spectra of raw ***Doxo***, ***MNPs@FA*** and ***Doxo*** loaded ***MNPs@FA***. The representative bands of ***MNPs@FA***, related to peptide bonds, at 1694 and 1626 cm^{-1} may be distinguished and associated to flexion vibration of C=O and stretching vibration of N-C=O respectively[19]. ***MNPs@FA-Doxo1*** spectrum exhibits a broad band at 1607 cm^{-1} that might be ascribe to the overlapping of signals of C=O stretching vibration from quinone and ketone groups of the ***Doxo*** and stretching vibration of N-C=O bond in ***MNPs@FA***[22]. Moreover, a slight shift of the signal regarding to flexion vibration of C=O of carboxylic groups on ***MNPs@FA*** surface from 1694 to 1687 cm^{-1} in ***MNPs@FA-Doxo1*** is observed. These findings could be associated to the ***FA*** and ***Doxo*** interaction potentially governed by electrostatic attraction[23]. The

presence of bands between 900 and 1300 cm^{-1}, that are absent in ***MNPs@FA*** spectrum, confirms the adsorption of ***Doxo*** on ***MNPs@FA*** surface[24,25]. Similar spectra were obtained analyzing ***MNPs@FA-Doxo0.5*** and ***MNPs@FA-Doxo2*** (supplementary material (a)). The spectrum of ***MNPs@FA-Doxo6*** (supplementary material (b)) shows broader bands associated to stretching vibration of the C-O, and C-O-C from ***Doxo*** than those observed in ***MNPs@FA-Doxo1*** spectrum. This result might be associated to the highest amount of absorbed drug at this condition of pH. The ***APTS-Doxo*** interaction was also evaluated to elucidate the role of FA in the drug adsorption. No evidences of drug incorporation were visualized in spectrum of ***MNPs-Doxo*** (suppl. mat. c) suggesting than the linking point to the ***MNPs*** surface would be the ***FA*** molecules.

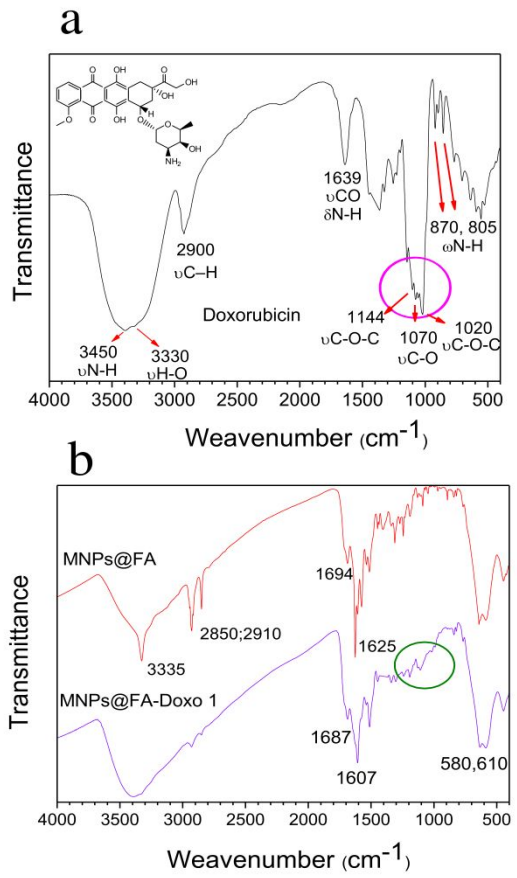

Fig. 1.(a) FTIR spectrum and chemical structure of pure Doxorubicin. (b) FTIR spectra of nanoparticles before and after loading of Doxo.

To further verify the presence of the therapeutic agent on ***MNPs@FA*** surface, UV-visible measurements were performed employing dispersions of 1mg nanoparticles/25mL BW. Supp. Mat (d) depicts UV-visible spectra of ***Doxo*** and ***FA*** solutions as a reference. The spectra of ***MNPs@FA***, and ***MNPs@FA-Doxo***'s dispersions are compared in supplementary material (e). It is observed that ***MNPs@FA***, ***MNPs@FA-Doxo1*** and ***MNPs@FA-Doxo6*** spectra exhibit an intense band around 283nm, ascribed to the π→ π* transitions of Pteridine (PT) ring[19], indicating the persistence of ***FA*** moieties in particle`s surface. A small shoulder at 485 nm could be distinguished in spectra of ***MNPs@FA-Doxo1*** and ***MNPs@FA-Doxo6*** included in figure (f) supplementary material, and may be assigned to the π→ π* transitions of drug molecules. Hence, this may consider as an extra proof of the presence of ***Doxo*** on the ***MNPs@FA***'s surface. The molar extinction coefficients (ξ) were calculated for both molecules, ***FA*** and ***Doxo***. The obtained values 26700 cm^{-1}.$L.mol^{-1}$ for ***FA*** and 10666 cm^{-1}.$L.mol^{-1}$ for ***Doxo*** are in agree with those found in the open literature[21]. Therefore, the higher amount of ***FA*** in the samples and its higher ξ in relation to the ***Doxo*** ,could be the reason of the low absorbance value visualized in the band at 485nm.

Table 1 includes the data of HD, by DLS and ζ and reveals that the incorporation of ***Doxo*** has an impact on the mean hydrodynamic diameter. The polydispersity index (PDI) for all measurements was lower than 0.5, indicating that all the samples are rather monodispersed particles in water[26].

Table 1. Hydrodynamic diameter (HD) and zeta potential (ζ) data of all the prepared formulations in aqueous dispersions. Doxo loading efficiency (%DLE) and loading capability (%DLC) as a function of the drug initially added to the MNPs.

Sample	Average Hydrodynamic Diameter (nm)	ζ(mV), pH:7.4	%DLE	% DLC
MAG	254.6 ± 9.8 PDI: 0.245±0.030	-35.5 ± 3.70	----------	----------
MNPs (MAG@APTS)	357.0 ± 8.2 PDI: 0.339 ± 0.025	-6.3 ± 1.70	----------	----------
MNPs-Doxo	762.2 ± 5.3 PDI: 0.431 ± 0.037	-2.3 ± 0.12	0.0	0.0
MNPs@FA	454.0 ± 12.6 PDI: 0.204 ± 0.090	-37.5 ± 0.20	----------	----------
MNPs@FA-Doxo0.5	890.4 ± 22.3 PDI: 0.139 ± 0.100	-30.1 ± 1.20	76.0± 3.8	6.9± 0,3
MNPs@FA-Doxo1	467.2 ± 2.9 PDI: 0.250 ± 0.036	-31.4 ± 0.15	62.4± 3.1	4.1± 0.2
MNPs@FA-Doxo2	699.1 ± 21.4 PDI: 0.100 ± 0.034	-31.6 ± 0.40	16.3±0.8	3.0±0.1
MNPs@FA-Doxo6	573.7 ± 20.2 PDI: 0.392 ± 0.029	-26.5 ± 0.10	95.0±1,9	7.5±0.1

It is well known that the HD of the nanoparticles should not be lower than 10nm. Indeed, these nanoparticles would be easily removed from the body being filtrated by the kidney. On the other hand, it is expected that larger nanoparticles would be quickly taken up by the liver, imparting short circulation time in blood[27]. In the case of high size solid tumor, a state of cellular hypoxia, initiates angiogenesis. These new tumor blood vessels are generally characterized by abnormalities such as high proportion of proliferating endothelial cells, pericyte deficiency and aberrant basement membrane formation leading to an enhanced vascular permeability[28]. In this context, particles ranging from 20 to 500 nm would be optimal when oncological pathology are considered[29].

The ***Doxo*** adsorption leads to slight variation on ζ, conserving negative surface charge with an almost constant magnitude independent on the concentration of loaded drug. This is commonly observed in MNPs systems[19].In this particular case, the data may be justified in terms of the kinds of interactions established between ***MNPs@FA*** surface and the ***Doxo***. When the adsorption is carried out without pH control , that is at pH of distilled water (MNPs@FA – Doxo0.5 to 2), the physical interactions like hydrogen bonding and hydrophobic ones, are the only feasible to promote the drug incorporation on magnetic surface. Due to their nature, these kinds of forces did not modify the surface charge of the magnetic nanosystems. As a difference, in the case of the adsorption performed at pH=6, electrostatic interactions between the

carboxylate group of the ***FA*** and amine protonated group of ***Doxo*** influenced the ζ values. The magnitude is lower in **MNPs@FA-Doxo6** (-26.1mV) due to the partial neutralization of negative charge by the drug amino groups. In all the cases, the magnitude of the ζ reveals that the dispersions are colloidal stable. The Scheme (a) of Supp. Mat. illustrates the analysis above described.

Figure (g) in supplementary material, includes TEM micrographies of ***MNPs@FA*** and ***MNPs@FA-Doxo1***. This last was taken as example of the influence of the drug on MNPs morphology. It is clearly observed that the original rod shape of ***MNPs@FA*** was modified during ***Doxo*** adsorption procedure leading to roughly spherical nanoparticles. This could be associated to the high surface tension of the ***Doxo*** solution on the ***MNPs@FA*** surface. This may be facilitated by the highly negative surface charge of ***MNPs@FA***. After adsorption of ***Doxo***, the nanorods structure disrupts leading to spherical MNPs dispersed in the drug matrix[30].

It is worth mention that the morphology of ***MNPs@FA*** observed in figure (g) Supp. Mat., is similar to the corresponding to the raw magnetic core previously reported[18]. Magnetization saturation value is not expected to suffer significant modifications regarding the value reached for raw magnetic core (~35emu/g) since the thickness of the layer formed by the modifiers is almost depreciable [18,19] .

Effect of different reaction parameters on the drug loading.

Doxo adsorption kinetic. Determination of optimal reaction time.

The optimal reaction time was evaluated using an indirect method reported elsewhere[31]. From figure (h) in supplementary material, it may infer that the amount of incorporated ***Doxo*** increases with the time, reaching the maximum value of 62.4± 3.1% at about 24h. Therefore, this time was adopted as optimum.

Influence of Doxo initial concentration on the %DLE

Data, listed in Table 1, reveal that the ratio ***Doxo/MNPs@FA*** = 0.5/10 (***MNPs@FA-Doxo0.5***), leads to the highest %DLE when the adsorption procedures is conducted at BW pH. It is also observed that increasing the nominal ***Doxo*** amount did not improve the loading efficiency. This behavior would be ascribed to the saturation of reactive sites on the ***MNPs@FA***[32]. From the recovered data, it would be possible assume that the highest amount of drug that could be adsorbed by a nanosystem is related to the nature of the carrier, the drug , and the type of interactions involved as well[33].

Influence of reaction pH on % DLE.

The highest %DLE is reached when the pH of the adsorption media was adjusted to 6 using PBS buffer. This result may be justified in terms of the mechanism of ***Doxo*** incorporation. Under this pH condition, the electrostatics interactions between COO^- groups of ***MNPs@FA*** (ζ at pH=6, -29.6mV)and NH_3^+ of ***Doxo***[34]are highly favored. It is worth to mention that, the presence of the band at 283nm in the UV-Vis spectra ascribed to PT ring group of ***FA***,was observed in almost all ***MNPs@FA-Doxo*** samples. This evidence reveals that the drug loading process would not affect the ***FA*** selective function[19].

Study of retention of MNPs@FA under the influence of a magnetic field.

One of the main objectives of using magnetic nanoparticles as theranostics lies in the fact that once injected into the bloodstream in a site near to the target place; they may be guided by applying an external magnetic field avoiding, or at least minimizing, severe side effects[15].

Data achieved from targeting assay is including in Fig.2 in terms of % of turbidimetric signal reduction as a function of the circulating time and was performed in conditions simulating the physiological ones. It is worth mention that a direct relationship between the concentrations of MNPs in dispersion (i.e. circulating) with the turbidimetric signal of the system at 440 nm was appreciated. Hence, a decrease in this parameter may be considered as a proof of the ***MNPs@FA*** accumulation on the TMP. The data included in the Fig.2 shows that the maximum amount of nanoparticles is retained during the first 500 s of experience. After this period of time, a less marked decrease was observed. According to the turbidity measurements, a decrease of around of 20%, with respect to the total amount of ***MNPs@FA*** circulating, was reached after 45min, revealing a reduction of ***MNPs@FA*** in dispersion by influence of the magnet stimuli.

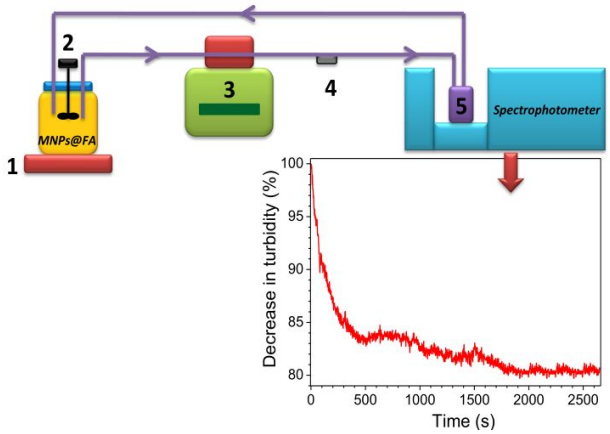

Figure 2. Reduction of the turbidimetric signal (%) vs time (s)

To better validate this data, quantitative measurement on the accumulated ***MNPs@FA*** mass was performed by AAS. The results suggest that almost 217±0.26 μg Fe were retained by the magnet after 45min, which represents the 21% with respect to the total amount of ***MNPs@FA*** circulating through the magnet targeting site. These findings completely agreed with those arising from the turbidimetric measurements. The *in vitro* evaluation of the magnet stimuli active targeting capability of magnetic nanoparticles has not been enough explored in current literature. It is worth mention that a scarce number of articles have been found in this concern and all of them are of recent publication. Besides, any of the reported works employed a FS with the capabilities of the device proposed within this work in terms of their easy handle and simplicity in the data acquisition[13]. For instance, K. Lee et al. explored the influence of thiol free groups on the magnetic retention capacity of nanoparticles [14].They compared data on targeting arising from *in vitro* flow system assays with those corresponding to *in vivo* studies. From the information provided in this article regarding to: i- the dosis administrated to the mice (12mg Fe/kg of mice), ii-the amount of Fe registered in the mice brain (1085 μg Fe/g) and, iii- the loaded efficiency of their MIONs (86.38 μg Doxo /g de Fe); a comparative analysis with our own data is possible to achieve. On this way a clear and preliminary perspective on the performance of our MNPs as theranostics may be reached. Such comparative data are included in Table 2.

Table 2. Comparative data related to the results reported by K. Lee et al. and the results obtained in this work using in vitro FS.

Sample	µg Fe retained in target site	Time of assay (min.)	% Fe retained	µg Drug (Doxo) in MNPs retained	Reference
MIONs	20	60	5.55	8.21	[14]
MNPs@FA	217	45	20	35-61	This work

In vitro MRI study

Iron oxide magnetic nanoparticles have been studied as T_2 MRI contrast agents because of their aptitude to decrease the T_2 relaxation time of the surrounding water protons in biological tissues.

In the present work, T_2 weighted images of a serie of dilutions of ***MNPs@FA*** were obtained in a whole body equipment of 1.5 T. It was observed that MRI signal intensity decreased considerably (images became darker) as the concentration of the nanoparticles increased from 0 to 0.1 mMFe. These results are depicted in Fig.3a. Fig.3b showing the T_2 decay curves, which indicates the lowering effect of magnetic nanoparticles in transverse relaxation time (T_2)[35]. For Fe concentration equal to 0, the curve seems too adopt a linear decay. These observations have been noted for other authors[36].

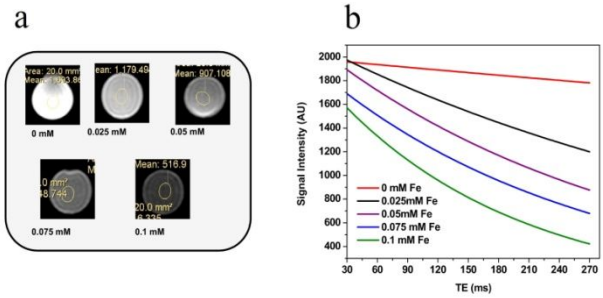

Figure 3. (a) T2 weighted images of MNPs@FA (TE=350 ms; TR=4000ms). (b) T2 curves obtained with different concentrations of ***MNPs@FA***

To quantify the efficiency of a contrast agent in shortening the T_2 relaxation time, the relaxivity r2 is commonly measured. This value is obtained by plotting the relaxation rate ($1/T_2$) vs the concentration of contrast agent (mM). The slope of the curve is the r_2 value. When plotting the relaxation rate vs iron concentration of ***MNPs@FA***, it was found that data follow a linear tendency, as it can be seen in figure (i) Suppl. Mat. (R-squared value: 0.97). The obtained r2 value was 47.8 ± 4 $mM^{-1}.s^{-1}$ at 1.5T)[37]

It has been reported that experimental parameters such as temperature, field strength and the medium have an impact in r2 determination. In addition to the experimental parameters, several factors have influence in the relaxivity value such as the size and shape of the nanoparticles, aggregation state and the number and size of ligands attached to the nanoparticle[38].

Besides, ***MNPs@FA*** has been designed to selectively accumulate in tumors that overexpress the folate receptor. On this way, the contrast effect could be improving due to the increment of ***MNPs*** in the target site. Other researchers have verified this behavior though *in vivo*/*in vitro* experiments. Jiang et al reported that in tumors that overexpress folate receptors, better contrast was achieved with folic acid conjugated magnetic nanoparticles compared with bare carboxymethyl dextran-coated magnetite[39].

The effect of the drug incorporation to MNPs' surface was also evaluated by comparing the T_2 values of ***MNPs@FA*** and ***MNPs@FA-Doxo*** for 0.2 (supplementary material (j)). The transverse relaxation time (T_2) evidenced insignificant changes, being slightly higher when ***Doxo*** is present. These results confirm that the presence of the drug did not significantly affect the T2 relaxation time of MNPs@FA.

In vitro Doxorubicin release

As it was commented in experimental section, a unique sample of nanoparticles was incubated, firstly in PBS buffer pH 7.4 and, subsequent in acetate buffer pH 4.9. This procedure was intended to simulate the pathway of MNPs once intravenous (IV) administrated. Therefore the pH 7.4 media simulate the nanocarriers in the bloodstream, whereas the pH 4.9 media emulates the access of nanocarriers to the tumoral cells[40].

For the best of these authors knowledge even when vast information about ***Doxorubicin*** release studies are abundant in open literature, any of them postulate the analysis here performed. In fact all the articles include two different procedures to evaluate the release of ***Doxo*** in each media[41,42]. Here, a better approximation of the *in vivo* conditions is possible by implementing this alternative and novel sequence.

Fig.4a shows ***Doxo*** release profile from ***MNPs@FA*** at pH 7.4. During the first 15 min. the ***Doxo*** released rapidly (burst effect), reaching a maximum of about 26.4±1.3 % during the first 45 min., remained almost constant for the next 15 min. The time of the experience was fixed at 60 min taking into account the data reported in ***Study of retention of MNPs@FA under the influence of a magnetic field*** section.

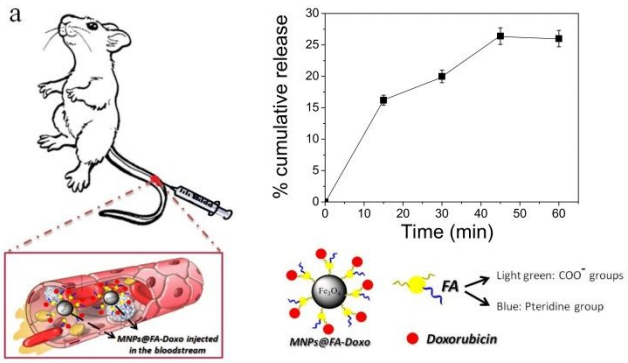

Figure 4. (a) Tentative scheme of nanoparticles in bloodstream once injected into the animal and the ***Doxo*** release profile from ***MNPs@FA-Doxo*** at pH 7.4.

After 1 h of release experience at pH 7.4 and 37 °C, ***MNPs@FA-Doxo*** were decanted by means of a Nd magnet and the PBS buffer was replaced for acetate buffer pH 4.9. Fig.4b shows the release profile of ***Doxo*** from ***MNPs@FA-Doxo*** at pH 4.9. A scheme of the entrance of the nanoparticles inside tumor cells and the release of ***Doxo*** is also presented. An increase of release of ***Doxo*** as a function of the time was observed, obtaining values of around 7.2 ± 0.7% of

cumulative release after 4 h of experience. The assay time was adopted based on data on the literature related to *in vitro* drug cellular uptake studies [43,44].

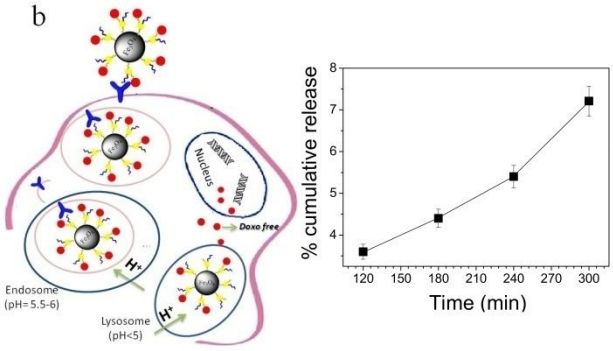

Figure 4(b) Scheme of the entrance of the nanoparticles inside tumor cells and the release profile of Doxo from ***MNPs@FA-Doxo*** at pH 4.9.

According to literature reports, higher and quicker drug release would be expected at low than at neutral pH[25]. However, in this study the presence of ***FA*** plays a role in the release kinetic. Jaimes-Aguirre et al. reported that ***FA*** moieties in nanoparticles of DOX-PLGA/γ-PGA-FA could reduce the release rate of ***Doxo*** because ***FA*** could intensify the chain entanglements, elongating the diffusion path of the drug. As a consequence the concentration gradient diminish, hindering the release[22]. Regards to the above mentioned, ***FA*** solubility in the studied media is an important factor influencing the release kinetic. Wu et al. informed that ***FA*** is soluble in aqueous media at pH between 6.0-9.8, but its solubility decreases when pH is 5.0 or lower[45]. In this context, it may infer that the highest ***Doxo*** release observed at pH=7.4 would be related not only to the release of ***Doxo*** per se, but also to the loss of ***FA*** conjugated with the drug. However, at pH=4.9 almost only the drug is released. Under acidic conditions, the amine ($-NH_2$) groups of ***Doxo*** and carboxilate (COO^-) groups of ***FA*** get protonated resulting in the partial dissociation of the interactions allowing the gradual release of the drug. Based on the work of James-Aguirre et al.[22], is important to remark that even when small amount of ***FA*** is missing at pH 7.4, the ***FA*** remained on the nanoparticles surface would be enough to the selectively uptake of this ones by the cells that overexpress folate receptors on their surface.

According to these results, roughly 7.2% of the administrated therapeutic agent would be able to reach the target site. In view of the reported data employing *in vivo* models, this doses would be enough to ensure the death of tumor cells.[14].

Conclusions

Nanotheranostics with potential to the treatment and diagnostic of oncological diseases have been achieved. The successful drug adsorption was assessed to achieve the therapeutic function. Characterization data revealed that all of the analyzed conditions ensured satisfactory ***Doxo*** adsorption on nanocarriers surface, being the mass ratio of Doxo/MNPs@FA = 0.5/1, pH=6 and 24 h of reaction the most suitable in terms of the loading efficiency. Turbidimetric and AAS measurements revealed a satisfactory response of the nanoparticles to accumulate in the magnet site under flow condition. The release achieved UV-visible data confirmed that suitable ***Doxo*** concentration would reach the tumor site allowing its therapeutic function.

Finally, MRI studies ensure that both, ***MNPs@FA*** and ***MNPs@FA-Doxo*** could be employed as efficient T_2 contrast agents.

Aiming to evaluate the *in vivo* toxicity and biocompatibility of ***Doxo***, ***MNPs@FA***, and ***MNPs@FA-Doxo***, an in deep study exploring the effect of a range of ***Doxo***, ***MNPs@FA***, and ***MNPs@FA-Doxo*** concentrations on an *in vivo* model, was already developed. The data achieved from this work takes part of a separate report[46].

Conflicts of interest

There are no conflicts to declare.

Acknowledgements

The authors acknowledge Lic. Adolfo Giles for the MRI technical support, Dra. Ma. Fernanda Horst for Fe measurements, the financial support of CONICET, ANPCyTand UNS (PGI24/ZQ09).

Notes and references

1 K. Webber and M. Friedlander, *Best Pract. Res. Clin. Obstet. Gynaecol.*, 2017, **41**, 126–138.
2 S. Smith and S. Prewett, *Obstet. Gynaecol. Reprod. Med.*, 2017, **27**, 206–212.
3 Y. Chen, L. Wang and J. Shi, *Nano Today*, 2016, **11**, 292–308.
4 E. Augustin, B. Czubek, A. M. Nowicka, A. Kowalczyk, Z. Stojek and Z. Mazerska, *Toxicol. Vitr.*, 2016, **33**, 45–53.
5 S. Shabalala, C. J. F. Muller, J. Louw and R. Johnson, *Life Sci.*, 2017, **180**, 160–170.
6 K. Cho, X. Wang, S. Nie, Z. Chen and D. M. Shin, *Clin. Cancer Res.*, 2008, **14**, 1310–1316.
7 F. Wang, M. Porter, A. Konstantopoulos, P. Zhang and H. Cui, *J. Control. Release*, 2017, **267**, 100–118.
8 M. Pei, X. Jia, X. Zhao, J. Li and P. Liu, *Carbohydr. Polym.*, 2018, **183**, 131–139.
9 F. Chen, G. Hableel, E. Ruike Zhao and J. V. Jokerst, *J. Colloid Interface Sci.*,2018,**521**,261-279.
10 M. Angelakeris, *Biochim. Biophys. Acta - Gen. Subj.*, 2017, **1861**, 1642–1651.
11 N. Schleich, C. Po, D. Jacobs, B. Ucakar, B. Gallez, F. Danhier and V. Préat, *J. Control. Release*, 2014, **194**, 82–91.
12 A. Shafei, W. El-bakly, A. Sobhy, O. Wagdy, A. Reda, O. Aboelenin, A. Marzouk, K. El, R. Mostafa, M. A. Ali and M. Ellithy, *Biomed. Pharmacother.*, 2017, **95**, 1209–1218.
13 P. Radon, N. Löwa, D. Gutkelch and F. Wiekhorst, *J. Magn. Magn. Mater.*, 2017, **427**, 175–180.
14 K. Lee, A. E. David, J. Zhang, M. C. Shin and V. C. Yang, *J. Ind. Eng. Chem.*, 2017, **54**, 389–397.
15 A. K. Hoshiar, T. A. Le, F. U. Amin, M. O. Kim and J. Yoon, *J. Magn. Magn. Mater.*, 2017, **427**, 181–187.
16 J. Park, N. R. Kadasala, S. A. Abouelmagd, M. A. Castanares, D. S. Collins, A. Wei and Y. Yeo, *Biomaterials*, 2016, **101**, 285–295.
17 Y. Wang, R. Zhao, S. Wang, Z. Liu and R. Tang, *Biomaterials*, 2016, **75**, 71–81.
18 P. Azcona, R. Zysler and V. Lassalle, *Colloids Surfaces A Physicochem. Eng. Asp.*, 2016, **504**, 320–330.
19 P. Azcona, I. López-Corral and V. Lassalle, *Colloids Surfaces A Physicochem. Eng. Asp.*, 2018, **537**, 185–196.
20 Y. Huang, K. Mao, B. Zhang and Y. Zhao, *Mater. Sci. Eng. C*, 2017, **70**, 763–771.
21 N. G. Yabbarov, G. a Posypanova, E. a Vorontsov, O. N. Popova and E. S. Severin, *Biochem. Biokhimiia*, 2013, **78**,

884–94.
22 L. Jaimes-Aguirre, E. Morales-Avila, B. E. Ocampo-García, L. A. Medina, G. López-Téllez, B. V. Gibbens-Bandala and V. Izquierdo-Sánchez, *Mater. Sci. Eng. C*, 2017, **76**, 743–751.
23 S. Yang, F. Lin, K. Tsai, M. Wei, H. Tsai and J. Wong, *Bioconjug. Chem.*, 2010, **21**, 679–689.
24 S. Kayal and R. V. Ramanujan, *Mater. Sci. Eng. C*, 2010, **30**, 484–490.
25 S. Sadighian and K. Rostamizadeh, *Colloids Surfaces B Biointerfaces*2014, **117**, 406–413.
26 M. Agotegaray, S. Palma and V. Lassalle, *J. Nanosci. Nanotechnol.*, 2014, **14**, 3343–3347.
27 M. P. M. M. Marciello, Y. Luengo, in *Pathology*, Elsevier Inc., 2006, pp. 667–694.
28 T. H. Stollman, T. J. M. Ruers, W. J. G. Oyen and O. C. Boerman, *Methods*, 2009, **48**, 188–192.
29 N. Schleich, P. Sibret, P. Danhier, B. Ucakar, S. Laurent, R. N. Muller, C. Jérôme, B. Gallez, V. Préat and F. Danhier, *Int. J. Pharm.*, 2013, **447**, 94–101.
30 B. Kundu, D. Ghosh, M. K. Sinha, P. S. Sen, V. K. Balla, N. Das and D. Basu, *Ceram. Int.*, 2013, **39**, 9557–9566.
31 M. A. Agotegaray and V. L. Lassalle, *IJCPA*,2014, **1**, 154–164.
32 E. Maltas, I. H. Gubbuk and S. Yildiz, *Biochem. Biophys. Reports*, 2016, **7**, 201–205.
33 Z. Liu, J. Liu, T. Wang, Q. Li, P. S. Francis, C. J. Barrow, W. Duan and W. Yang, *J. Mater. Chem. B*, , DOI:10.1039/C7TB03063K.
34 A. Neacșu, *Thermochim. Acta*, 2018, **661**, 51–58.
35 E. Illés, M. Szekeres, E. Kupcsik, I. Y. Tóth, K. Farkas, A. Jedlovszky-Hajdú and E. Tombácz, *Colloids Surfaces A Physicochem. Eng. Asp.*, 2014, **460**, 429–440.
36 F. A. Cardona, E. S. Urquiza, P. de la Presa, S. H. Tobón, U. Pal, P. H. Fraijo, M. J. Yacaman, J. D. Lozada Ramírez, R. Ivkov, A. Angulo-Molina and M. Á. Méndez-Rojas, *RSC Adv.*, 2016, **6**, 77558–77568.
37 V. Sreeja, K. N. Jayaprabha and P. A. Joy, *Appl. Nanosci.*, 2015, **5**, 435–441.
38 N. Lee and T. Hyeon, *Chem. Soc. Rev.*, 2012, **41**, 2575–2589.
39 Q. L. Jiang, S. W. Zheng, R. Y. Hong, S. M. Deng, L. Guo, R. L. Hu, B. Gao, M. Huang, L. F. Cheng, G. H. Liu and Y. Q. Wang, Appl. Surf. Sci., 2014, 307, 224–233
40 Z. Wang, C. Zhou, J. Xia, B. Via, Y. Xia, F. Zhang, Y. Li and L. Xia, *Colloids Surfaces B Biointerfaces*, 2013, **106**, 60–65.
41 S. Mehrad Fard, N. Farhadian, T. Rohani Bastami, M. Ebrahimi, M. Karimi and A. Allahyari, *J. Drug Deliv. Sci. Technol.*, 2017, **38**, 116–124.
42 A. Pourjavadi, S. H. Hosseini, M. Alizadeh and C. Bennett, *Colloids Surfaces B Biointerfaces*, 2014, **116**, 49–54.
43 E. Augustin, B. Czubek, A. M. Nowicka, A. Kowalczyk, Z. Stojek and Z. Mazerska, *Toxicol. Vitr.*, 2016, **33**, 45–53.
44 J. Mosafer, K. Abnous, M. Tafaghodi, A. Mokhtarzadeh and M. Ramezani, *Eur. J. Pharm. Biopharm.*, 2017, **113**, 60–74.
45 Z. Wu, X. Li, C. Hou and Y. Qian, *J. Chem. Eng. Data*, 2010, **55**, 3958–3961.
46 D. Igartúa, P. Azcona, C. Martinez, S. del V. Alonso, V. Lassalle and M. J. Prieto, *Toxicol. Appl. Pharmacol.*, 2018, **358**, 23–34.

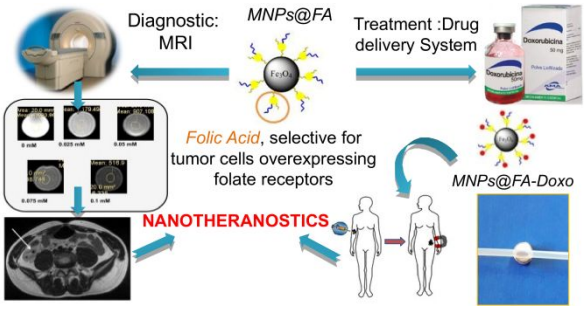

This work reports an overview of required *in vitro* assays to evaluate nanotheranostics concrete applications perspectives